International Journal of Biological Engineering and Agriculture
ISSN: 2833-5376
Volume 03 Number 03 (2024)
Impact Factor: 9.51
SJIF (2023): 3.916

www.inter-publishing.com

Article

Utilizing Spectral Reflectance for Separating Salinity-Affected Sedimentary Soil Units and Predicting Some of Their Properties in Northern Basra Governorate

Mustafa Saleh Ali Al-Mayahi[1], Salah Mahdi Sultan Al-Atab[2]

1. Basra Governorate Agriculture Directorate, Iraq
* Correspondence: pgs.mustafa.saleh@uoBasrahh.edu.iq
2. University of Basra, College of Agriculture, Department of Soil Sciences and Water Resources, Iraq

Abstract: The study aimed to separate soil units and predict some of their properties using geomatics techniques and spectral reflectance analysis in the northern part of Basra Governorate in southern Iraq through spectral reflectance study. Chemical properties (Ece, pH, O.C, CEC, $CaCO_3$, ESP, CEC) and physical properties (particle size distribution) were studied, in addition to the assumed composition of prevailing salts in the study area. Three sedimentary soil units were identified (river terraces, river basins, and marshes). Furthermore, there were significant correlations between spectral reflectance of spectral bands 4 and 5 and soil organic carbon content of 0.75 and 0.8, respectively, and with other spectral bands except bands 2 and 8. There were significant relationships between other properties and different spectral bands. Notably, there were no significant correlations between pH, ESP, $CaCO_3$, $CaSO_4$, and all spectral bands. The most predictable soil property through spectral reflectance is the soil's organic carbon content. Bands 4 and 5 are the most commonly used in soil science, especially in agriculture.

Keywords: Spectral reflectance, spectral bands, DEM, Alluvial soils

Citation: Al-Mayahi, M. S. A., & Al-Atab, S. M. S. Utilizing Spectral Reflectance for Separating Salinity-Affected Sedimentary Soil Units and Predicting Some of Their Properties in Northern Basra Governorate. International Journal of Biological Engineering and Agriculture 2024, 3(3), 42-54.

Received: 4th March 2024
Revised: 11th March 2024
Accepted: 17th March 2024
Published: 24th March 2024

1. Introduction

Spectral reflectance has become an increasingly important focus in soil characterization as it provides a valuable means to understand the various properties of soil. In sedimentary soils known for their fertility found in terraces, river basins, and marshes, spectral reflectance provides important insights into their formation processes and composition. Spectral reflectance is closely linked to soil properties and conditions, including soil organic matter content, moisture content, texture, and chemical composition. These properties significantly influence the spectral reflectance of soil, especially in soil types such as sedimentary soils that exhibit unique spectral reflectance properties associated with their diverse characteristics [1].

The relationship between soil spectral reflectance and its physical and chemical properties is a highly important topic, and the feasibility of estimating soil properties through spectral reflectance data aims to facilitate the use of spectral data in soil analysis by linking soil properties to different spectral bands [2]. Studies have shown that the composition of sedimentary soils, greatly influenced by their deposition source, can be closely observed through the study of their spectral reflectance patterns. Spectral reflectance data can identify surface property variations indicating diversity in the origin of these soils [3].

The spectral reflectance of soil is influenced by its diverse composition, particularly in sedimentary soils due to deposition and weathering processes that define these natural landscapes [4].

Laboratory-based analyses were conducted to explore the spectral effects of salinity and gypsum addition on Brazilian sedimentary soils, resulting in significant variations in spectral reflectance. These observations are crucial for understanding the impact of salt content on the spectral reflectance of sedimentary soils, which is essential for remote sensing applications in mapping and soil classification [5]. Furthermore, variations in soil properties across natural landscapes of sedimentary soils can affect recorded spectral reflectance data, influencing how these soils are managed and utilized in agricultural practices [6]. The sensitivity of sedimentary soils to environmental and management practices, such as fertilization and irrigation, was observed through changes in soil spectral reflectance. Research indicates that agricultural practices have significant effects on the spectral properties of sedimentary soils, from the original soil structure to its composition. Understanding the impact of soil composition on plant spectral reflectance, such as wheat, is crucial for accurate interpretation of remote sensing data and its applications in precision agriculture, land use planning, and conservation efforts [7]. The application of spectral reflectance in studying the properties of sedimentary soils not only enhances knowledge of their physical and chemical composition but also facilitates the development of models and techniques for soil classification, crop monitoring, and precise evaluation - essential elements in sustainable land management practices. In this context, this study aims to utilize spectral reflectance in understanding and identifying soil properties and delineating soil units in northern Basra Governorate.

2. Materials and Methods

2.1. Study area

The study area is located in the northern part of Basra Governorate in the southeastern part of Iraq. It lies between longitudes 47° 24' and 47° 61' east and latitudes 30° 68' and 31° 07' north. It is bordered by Maysan Governorate to the north, Al-Haritha District to the south, Shatt al-Arab and Tigris River to the east, and Al-Zubair District to the west. The study area encompasses the northern part of Basra Governorate, including the alluvial plain and the southern part of the Western Desert, with an estimated area of 827 km², equivalent to 330,878.07 dunums.

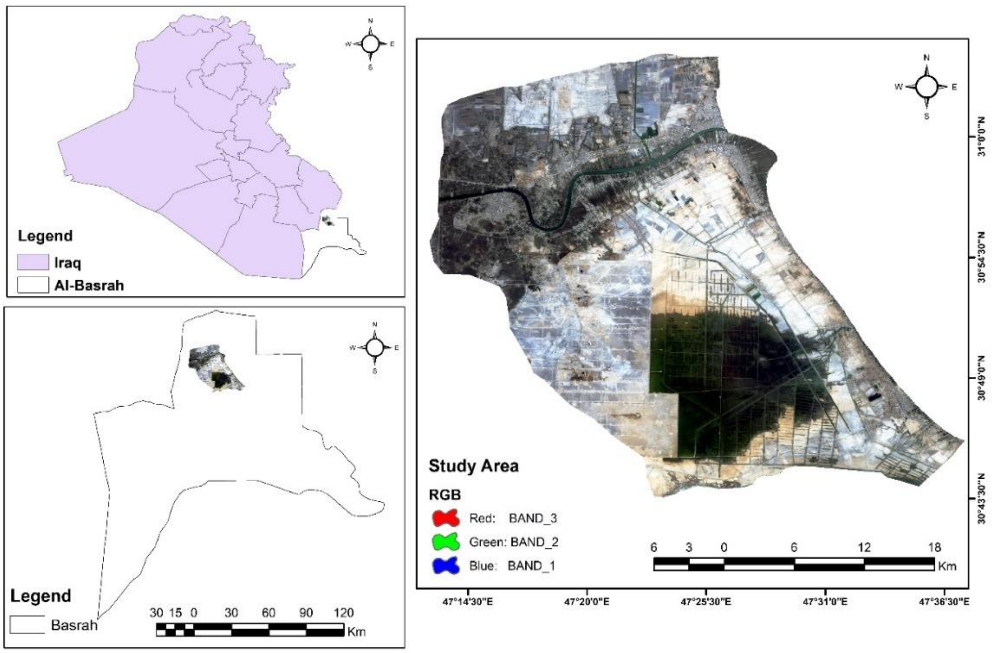

Figure 1. Study area

2.2. Climate

The study area falls within a hot and arid desert climate, with an annual rainfall of 191.9 mm. The rainfall is irregularly distributed throughout the eight months, accompanied by high annual average temperatures. The annual average temperature is around 28.9°C, with peak temperatures reaching 48°C in July. Therefore, the soils in the study area exhibit a Hyperthermic thermal regime due to the annual temperature average exceeding 22°C, and a Torric Aridic moisture regime, indicating arid conditions throughout the year [8].

2.3. Desk Work

This phase involved several important processes, including:

1) Satellite imagery

Satellite imagery was downloaded from the international web network, specifically from the official website of the US Geological Survey (USGS) for the Landsat 8 satellite, captured on 25/10/2022, covering the study area. The compressed image file contained eleven spectral bands with spatial discrimination capabilities.

- Subset image extraction: The study area was delineated on the resulting satellite image, and then a subset of the study area was extracted for each band of the satellite imagery.

2) Digital processing of satellite imagery

Digital processing of satellite imagery was conducted using a series of mathematical algorithms through software such as Arc 10.4.1 and ERDAS 2014, including:

- Layer stack spectral bands: Spectral bands 2, 3, 4, 5, and 8 were merged using ERDAS software and the Merge resolution command to create a single spectral band with high discriminatory capabilities. This process aimed to enhance spatial discrimination and prepare the imagery for digital processing and identification of land features. Additionally, these bands can be used in both unsupervised and supervised classification processes.
- Atmospheric correction: The atmosphere contains various gases, including oxygen, nitrogen, ozone, carbon dioxide, water vapor, smoke, and dust. These gases affect certain components of the electromagnetic radiation as it passes through the atmosphere, leading to scattering or absorption. For instance, most blue light is scattered, and some electromagnetic radiation is absorbed by gases like carbon dioxide and oxygen. According to Wu (2011) [9], signals recorded by various satellite sensor devices are affected by atmospheric scattering and absorption. It is essential to remove these effects, especially when using satellite images for multiple dates or land cover classification purposes. Converting Digital Numbers to Reflectance values is a crucial process in reducing the impacts of absorption and scattering of electromagnetic energy in satellite images, enhancing the accuracy of classifying different land cover types using the following equation.

$L\lambda = ML*Qcal + AL$ ……. ……(1)

where:

$L\lambda$ = Spectral radiance (W / (m2 * sr * μm))

ML = Radiance multiplicative scaling factor for the band (RADIANCE_ MULT_ BAND_n from the metadata).

AL = Radiance additive scaling factor for the band (RADIANCE_ ADD_ BAND_ n from the metadata).

Qcal = Level 1-pixel value in DN

$\rho\lambda' = MP*Qcal + AP$ ……. (2)

where:

$\varrho\lambda'$ = Top-of-Atmosphere Planetary Spectral Reflectance, without correction for solar angle. (Unitless)

MP = Reflectance multiplicative scaling factor for the band (REFLECTANCEW_ MULT_ BAND_n from the metadata).

AP = Reflectance additive scaling factor for the band (REFLECTANCE_ ADD_ BAND_N from the metadata).

Q cal = Level 1-pixel value in DN

Note: that $\varrho\lambda'$ is not true TOA Reflectance, because it does not contain a correction for the solar elevation angle. This correction factor is left out of the level 1 scaling at the users' request; some users are content with the scene-center solar elevation angle in the metadata, while others prefer to calculate their own per-pixel solar elevation angle across the entire scene. Once a solar elevation angle is chosen, the conversion to true TOA Reflectance is:

$\varrho\lambda = \varrho\lambda' / \sin(\theta)$ ……. (3)

where:

$\varrho\lambda$ = Top-of-Atmosphere Planetary Reflectance. (Unitless)

θ = Solar Elevation Angle (from the metadata, or calculated).

The solar elevation angle is given in degrees and the date is in the format "YYDDDHH" where the 3 "D" digits denote the day of the year. Keep in mind that the sine function within Arc Map requires the solar elevation angle to be in radians instead of degrees. Convert from degrees to radians using.

Radians = (degrees * π) /180^o …… (4)

3) Downloading the Digital Elevation Model (DEM)

Digital elevation model (DEM) files were utilized in a Geographic Information System (GIS) environment to produce digital elevation maps and land topography. These files were obtained from the US Geological Survey (USGS) website with a resolution of 25x25 meters. The method followed for extracting slope characteristics from the satellite data and the DEM was outlined in the software guide.

- Outlier value processing – fill: One of the tools in the Hydrology analysis toolbox is the Fill command, which fills unexpected depressions (sinks) in the digital elevation data. These sinks are cells with significantly lower elevation values compared to their neighboring cells. These unexpected depressions are often the result of flaws in the DEM, and therefore, they need to be removed to create a new DEM file free of depressions.
- Contour map: A contour map of the area was derived in linear format as a Shapefile with contour intervals of 100 meters.
- Soil unit separation: Several exploratory visits were conducted in the study area to understand the land use patterns. Using ArcGIS 10.4.1 software, a Shapefile was created based on the digital elevation model (DEM), spectral reflectance data, and some spectral indices used. The study area was divided into three units based on the DEM, spectral reflectance, and spectral index values for each unit. This division helped in determining the boundaries of each unit, extracting and separating each soil unit, and calculating the area of soil units in the study area.

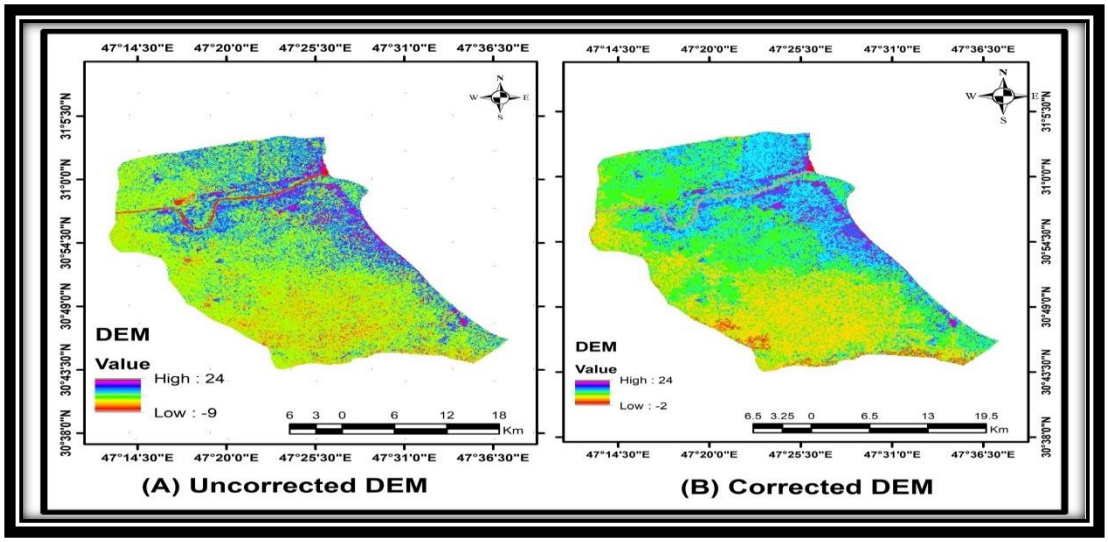

Figure 2. Digital Elevation Model (DEM)

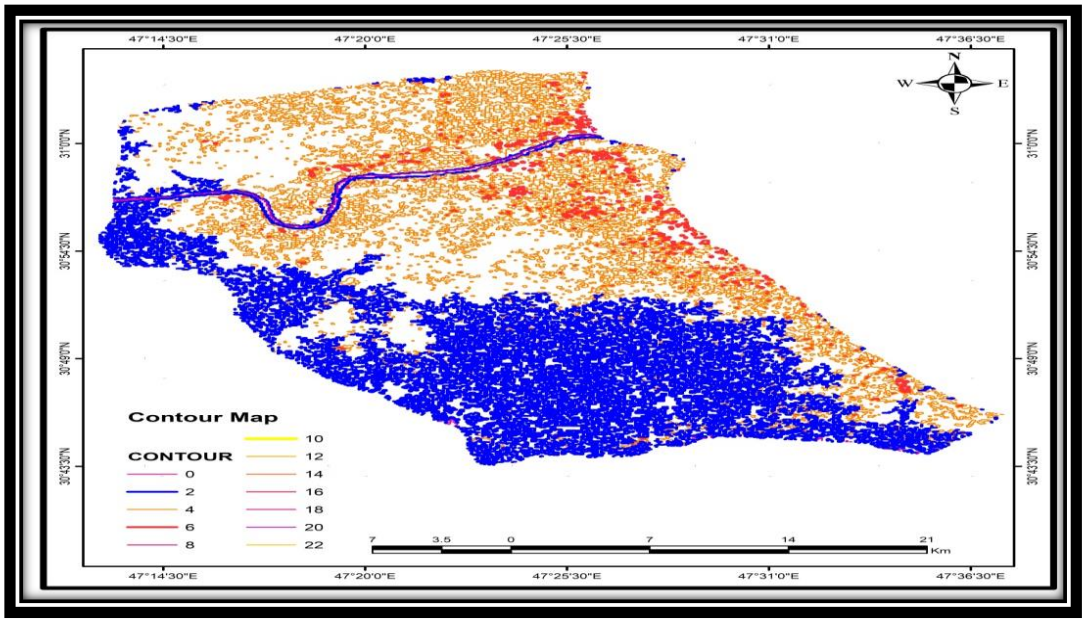

Figure 3. Contour map

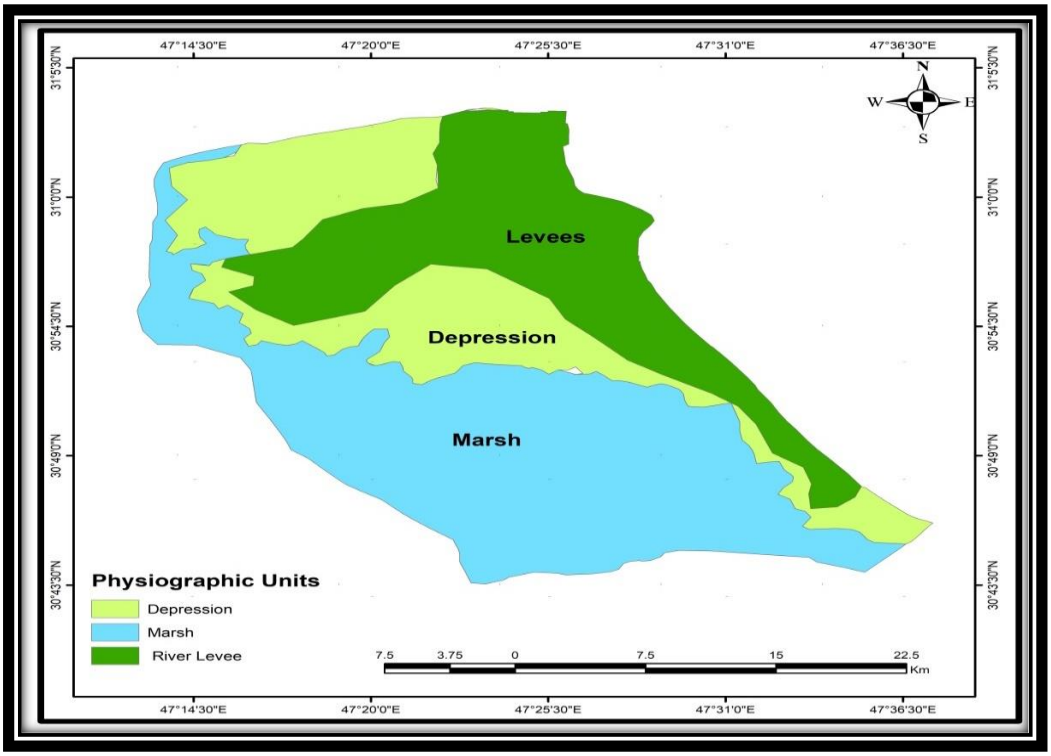

Figure 4. Separation soil unit

The study area is located in the southern part of the alluvial plain. Three physiographic units were identified:

1) Unit of the River Levees
2) Unit of the Depression
3) Unit of the Marsh

These physiographic units represent formations in the alluvial plain consisting of water deposits resulting from the Tigris, Euphrates, and Shatt al-Arab rivers during flood events.

3. Results and Discussion

3.1. Spectral reflectance

The study utilized Landsat 8 spectral reflectance for the study area, with results presented in Table 1 showing the relationship between spectral reflectance and soil units. A decrease in spectral reflectance was observed in band 2, ranging between 0.10676 and 0.14429, followed by a value of 0.13190 for Pedon 6 in the River Basin unit, Pedon 4 in the River Valley unit, and Pedon 12 in the Marsh unit consecutively. In band 3, values ranged between 0.11461 for Pedon 6 and 0.14962 for Pedon 12, and 0.15972 for Pedon 4 successively.

Regarding band 4, values ranged between 0.11571 for Pedon 6 in the River Basin unit, and the highest value was 0.17384 for Pedon 4 in the River Valley unit, followed by 0.16211 for Pedon 12 in the Marsh unit. For band 5, values ranged between 0.11397 for Pedon 5 in the River Valley unit, and 0.13843 for Pedon 6 in the River Basin unit. The highest reflectance value was for Pedon 12 in the Marsh unit at 0.18784, and for Pedon 4 in the River Valley unit at 0.19022, respectively.

As for band 6, values ranged between 0.11836 for Pedon 5 in the River Valley unit, and 0.19872 for Pedon 3 in the River Basin unit, with the highest value being 0.20037 for Pedon 12 within the Marsh unit. Regarding band 7, its values ranged between 0.12618 for Pedon 6 in the River Basin unit, and the highest reflectance was 0.20126 for Pedon 9 within

the Marsh unit. Lastly, for band 8, values ranged between 0.03464 for Pedon 5 in the River Valley unit, and the highest value was 0.03914 for Pedon 12 in the Marsh unit.

Table 1. Spectral reflectance values for landsat-8 satellite bands for the studied pedons in 2022

	Spectral Reflectivity Values						
Pedons	**B2**	**B3**	**B4**	**B5**	**B6**	**B7**	**B8**
P1	0.12622	0.13809	0.14542	0.14756	0.17588	0.16916	0.03861
P2	0.13063	0.13330	0.14250	0.16595	0.18892	0.18298	0.03814
P3	0.10866	0.14897	0.15080	0.16784	0.14757	0.12785	0.03767
P4	0.14429	0.15972	0.17384	0.19022	0.19872	0.18739	0.03767
P5	0.11468	0.14110	0.12654	0.11397	0.11836	0.11691	0.03464
P6	0.10676	0.11461	0.11571	0.13690	0.13843	0.12618	0.03566
P7	0.12506	0.13939	0.14834	0.16933	0.17883	0.16540	0.03814
P8	0.12469	0.13661	0.14643	0.15596	0.16889	0.16164	0.03732
P9	0.13248	0.14656	0.15538	0.17170	0.20126	0.19598	0.03661
P10	0.12190	0.13350	0.14139	0.15898	0.17079	0.16124	0.03912
P11	0.12766	0.14248	0.15431	0.18784	0.19017	0.18480	0.03844
P12	0.13190	0.14962	0.16211	0.19752	0.20037	0.19018	0.03914

From the above results, a decrease in spectral reflectance values for the spectral bands is observed. Pedons 1, 5, and 6 recorded the lowest spectral reflectance values across all spectral bands. This is because these pedons are located in cultivated areas with distinct vegetation cover and low soil salt content, leading to decreased spectral reflectance values due to the absorption of electromagnetic radiation by the higher organic carbon content in the soil.

The study results also indicate that the River Basin unit exhibits the lowest spectral reflectance values across the spectral bands, while the River Valley unit shows the highest spectral reflectance values in bands 2, 3, 4, and 5. As for the Marsh unit, it has the highest spectral reflectance values in bands 6, 7, and 8.

3.2. Particle size distribution

The Table 2 illustrates the relationship between soil particle size distribution and spectral reflectance. There was a significant negative correlation between sand content and spectral reflectance for bands 2, 4, 6, 7, and 8. This decrease in spectral reflectance with sand content reduction is attributed to the influence of other soil properties, such as surface roughness affecting the reflective properties of the soil. Additionally, the decrease in spectral reflectance with lower sand content is influenced by factors like lower calcium content and higher organic carbon content in certain soil units compared to others.

Table 2. Correlation between spectral reflectance and some soil properties for surface horizons of selected pedons in the study area

	Bands	PH	EC	ESP	$CaCO_3$	$CaSO_4$	O.C	CEC	SAND	CLAY	SILT
B2	Pearson Correlation	.325	.053	-.006	.114	.203	-.517	-.418	-.628*	.098	.445
	Sig. (2-tailed)	.303	.869	.985	.725	.527	.085	.176	.029	.763	.147
	N	12	12	12	12	12	12	12	12	12	12
B3	Pearson Correlation	.349	.457	-.549	.402	.313	-.650*	-.702*	-.375	-.299	.584*
	Sig. (2-tailed)	.266	.136	.065	.196	.322	.022	.011	.230	.345	.046
	N	12	12	12	12	12	12	12	12	12	12
B4	Pearson Correlation	.256	.465	-.178	.447	.347	-.751**	-.657*	-.524	-.009	.452
	Sig. (2-tailed)	.423	.127	.580	.145	.270	.005	.020	.080	.977	.140
	N	12	12	12	12	12	12	12	12	12	12
B5	Pearson Correlation	.139	-.608*	.085	.563	.531	-.801**	-.518	-.474	.213	.211
	Sig. (2-tailed)	.666	.036	.792	.057	.076	.002	.084	.119	.506	.511
	N	12	12	12	12	12	12	12	12	12	12
B6	Pearson Correlation	.265	.274	.202	.247	.352	-.687*	-.351	-.681*	.276	.331
	Sig. (2-tailed)	.405	.389	.529	.439	.261	.014	.264	.015	.386	.294
	N	12	12	12	12	12	12	12	12	12	12
B7	Pearson Correlation	.343	.155	.163	.114	.312	-.636*	-.298	-.697*	.253	.365
	Sig. (2-tailed)	.274	.631	.614	.723	.324	.026	.347	.012	.428	.244
	N	12	12	12	12	12	12	12	12	12	12
B8	Pearson Correlation	.320	.412	.086	.381	.401	-.533	-.139	-.491	.651*	-.169
	Sig. (2-tailed)	.310	.183	.789	.221	.196	.074	.667	.105	.022	.599
	N	12	12	12	12	12	12	12	12	12	12

*Correlation is significant at the 0.05 level (2-tailed).

**. Correlation is significant at the 0.01 level (2-tailed).

3.3. Soil sand Content

Table 2 shows a significant negative correlation between soil silt content and spectral reflectance for band 3. Generally, there was a decrease in spectral reflectance with an increase in soil silt content in the study area. This decrease can be attributed to the presence of salts and saline soils, such as magnesium chloride, which increase the soil's ability to absorb light due to its wet, sticky, and dark characteristics, leading to lower spectral reflectance.

3.4. Soil silt content

It is noted from Table 2 a significant correlation between soil silt content and the spectral reflectance values of soil with spectral band 3 only, which was 0.584*. However, there is a correlation with other spectral bands as well. Generally, a decrease in reflectance values with an increase in soil silt content for the soils in the study area is observed. This is attributed to the interference and impact of other soil components. The high salt content in the study area and the prevalence of salts conducive to this type of soil (saline soils)

such as magnesium chloride increase the soil's ability to absorb light energy due to the moist, sticky surface and dark color characteristic of these soils, leading to a decrease in spectral reflectance values [10].

3.5. Soil clay content

From Table 2, a significant correlation is observed between clay content and spectral reflectance values of soil for spectral band 8, reaching 0.651*. Generally, it is observed that reflectance values increase with an increase in clay content for the soils in the study area and decrease at lower contents for some soils. The smaller soil particle diameter increases its reflectance, while an increase in particle diameter decreases spectral reflectance. Finer texture soils are more reflective than coarser texture soils due to the smoother surface of fine soil particles. Moreover, the increase in reflectance with clay content may be attributed to the influence and interaction of other soil properties. These findings are consistent with those found by Demattê et al. (2016) [11].

3.6. Electrical Conductivity (Ece)

The results in Table 2 indicate that the highest correlation coefficient between soil electrical conductivity and spectral reflectance values of Landsat 8 satellite was observed with spectral band 5, reaching 0.60. Despite the statistically significant relationship with spectral band 5, no correlation was observed with other spectral bands. Additionally, there was no increase in spectral reflectance values of the studied soil with an increase in electrical conductivity values. This result suggests a high proportion of soluble salts in such saline soils, affecting their optical and spectral properties. These soils are characterized by the prevalence of salts such as magnesium chloride, enhancing their ability to absorb electromagnetic radiation. Due to their wet, sticky, and dark-colored surface, these soils exhibit low reflectance values despite the high salinity content [12], [13].

3.7. Exchangeable Sodium Percentage (ESP)

The results in Table 2 revealed the highest correlation between exchangeable sodium percentage and spectral reflectance for Landsat 8's band 3, reaching -0.549. Clear differences in correlation coefficients were observed due to the small measurement area, with band 3 showing the highest sensitivity to dark-colored soils. This aligns with previous studies highlighting the impact of soil properties on spectral reflectance.

3.8. Total mineral carbonate content

Table 2 indicates a significant correlation between soil mineral carbonate content and spectral reflectance for Landsat 8's band 5, reaching 0.563. Spectral reflectance values generally increased with higher carbonate content but decreased overall. This is due to the influence of other soil properties, such as high soluble salt content, organic carbon content, and soil moisture, leading to increased light absorption and decreased reflectance.

3.9. Soil gypsum content

The results in Table 2 revealed that the highest correlation coefficient between soil gypsum content and spectral reflectance values of Landsat 8 satellite was observed with spectral band 5, reaching 0.531. The results indicated a positive relationship between gypsum content and reflectance; however, the low gypsum content and the lack of significant variation in gypsum proportions, in addition to the presence of carbonate minerals in the studied sites, led to a decrease in the correlation values. It was observed that very high gypsum content in the soil resulted in higher average reflectance compared to other soil properties, which is consistent with findings reported by Dwivedi (2017) [14].

3.10. Soil organic carbon content

The results in Table 2 demonstrate a significant correlation with all spectral bands, with the highest correlation observed between soil organic carbon content and spectral

reflectance of Landsat 8 satellite for all spectral bands, reaching values of -0.52, -0.65, -0.751, -0.801, -0.69, -0.64, and -0.533 for spectral bands 2, 3, 4, 5, 6, 7, and 8, respectively. This may be attributed to the quantity of organic carbon in the soil, which plays a crucial role in the spectral response of the soil. An increase in organic carbon content leads to higher spectral absorption. Organic materials are associated with the spectral reflectance properties of satellite imagery, especially the clay fraction ratio in the soil. From the above results, it is possible to predict the amount of organic carbon in the soil using Landsat 8 sensor with good spatial accuracy in open areas, consistent with findings by Castaldi (2021) [15]; Zeng et al. (2022) [16].

3.11. Cation Exchange Capacity (CEC)

Table 2 shows a significant negative correlation between cation exchange capacity and spectral reflectance for soil units in the study area, with values ranging from -0.518 to -0.702 for bands 3, 4, and 5. This inverse relationship is attributed to the high organic carbon content in soil and the interaction with other soil components like clay and silt, rather than the cation exchange capacity alone.

3.12. The predominant salts

The results in Table 3 indicate the prevalence of sodium chloride and magnesium chloride salts in the study area, observed across all surface horizons of the pedons. These salts are characterized by their high solubility. Additionally, magnesium chloride has the ability to absorb atmospheric moisture, thereby significantly reducing spectral reflectance. This reduction occurs despite the high salinity of the soil and its high content of carbonate minerals. Moreover, sodium chloride salts accumulate in the surface layers.

Table 3. Predominant salts in the surface layer of studied pedons

Salt type Pedons	$Ca(HCO_3)_2$	$CaSO_4$	$MgSO_4$	$CaCl_2$	$MgCl_2$	KCl	NaCl
	Meq L^{-1}						
P1 AP	5.57	47.43	-	17.78	182	3.75	319.59
P2 A	11.31	78.35	32.92	-	157.07	6.98	539.59
P3 A	26.88	80.34	-	22.22	254	12.89	446.67
P4 A	3.33	78.46	-	34.21	222	7.9	814
P5 AP	2.3	46.85	18.25	-	255.75	3.82	254.22
P6 AP	3.66	80	-	36.34	96	3.83	112.17
P7 A	3.33	27.08	-	53.25	282	11.86	106.14
P8 A	2.67	27.08	-	63.58	114	4.27	382
P9 A	1.4	46.4	65.86	-	180	5.6	209.58
P10 A	3.28	65.3	-	13.06	144	7.53	402.09
P11 A	9.56	82.04	-	9.18	200	9.1	492.54
P12 A	3	124	-	84.5	112	12.26	649

4. Conclusion

The spectral reflectance results indicate a decrease in spectral reflectance values for the spectral bands. Pedons 1, 5, and 6 recorded the lowest spectral reflectance values for all spectral bands, as these pedons are located in cultivated areas with distinct vegetation cover. The decrease in soil salt content led to a decrease in spectral reflectance values, along with an increase in soil organic carbon content, which absorbs electromagnetic radiation, thus reducing spectral reflectance.

Pedon units classified as River Basin exhibit the lowest reflectance values in the spectral bands, whereas those classified as River Beds show the highest reflectance values in

bands 2, 3, 4, and 5. Marshland units had the highest reflectance values in bands 6, 7, and 8.

Significant correlations were observed between soil greens content and soil spectral reflectance values in only spectral band 3, with a correlation coefficient of 0.584*. Similarly, significant correlations were observed between soil clay content and spectral reflectance values in only spectral band 8, with a correlation coefficient of 0.651*. Negative significant correlations were observed between soil sand content and spectral reflectance values in bands 2, 6, and 7, with correlation coefficients of 0.628*, 0.681*, and 0.697*, respectively.

The study results demonstrate that soil organic carbon content is the most predictable soil property using spectral reflectance. High significant correlations were found between spectral bands 4 and 5 with correlation coefficients of 0.751* and 0.801*, respectively, as well as with bands 3, 6, and 7 with correlation coefficients of 0.65*, 0.678*, and 0.636*, respectively. Additionally, significant negative correlations were found between spectral reflectance and cation exchange capacity, with a correlation coefficient of 0.657* in band 4, and between spectral reflectance and electrical conductivity, with a correlation coefficient of 0.608* in band 4.

REFERENCES

[1] A. K. Sinha, "Spectral reflectance characteristics of soils and its correlation with soil properties and surface conditions," *Journal of the Indian Society of Remote Sensing*, 1986, doi: 10.1007/BF03007217.

[2] E. B. Dor, C. Ong, and I. C. Lau, "Reflectance measurements of soils in the laboratory: Standards and protocols," *Geoderma*, 2015, [Online]. Available: https://www.sciencedirect.com/science/article/pii/S0016706115000038

[3] A. K. Batchily, D. F. Post, R. B. Bryant, and ..., "Spectral reflectance and soil morphology characteristics of Santa Rita Experimental Range soils," *Santa Rita Experimental …*, 2003, [Online]. Available: https://www.fs.usda.gov/research/treesearch/download/36022.pdf

[4] H. J. Liu, B. Zhang, Y. Z. Zhang, K. S. Song, and ..., "Soil taxonomy on the basis of reflectance spectral characteristics," *Guang pu xue yu …*, 2008, [Online]. Available: https://europepmc.org/article/med/18536428

[5] L. C. J. Moreira, A. S. Teixeira, and L. S. Galvão, "Laboratory salinization of Brazilian alluvial soils and the spectral effects of gypsum," *Remote Sens (Basel)*, 2014, [Online]. Available: https://www.mdpi.com/2072-4292/6/4/2647

[6] M. Mzuku, R. Khosla, and R. Reich, "Bare soil reflectance to characterize variability in soil properties," *… in Soil Science and Plant Analysis*, 2015, doi: 10.1080/00103624.2015.1043463.

[7] E. Prudnikova, I. Savin, G. Vindeker, P. Grubina, and ..., "Influence of soil background on spectral reflectance of winter wheat crop canopy," *Remote Sens (Basel)*, 2019, [Online]. Available: https://www.mdpi.com/2072-4292/11/16/1932

[8] S. Al-Atab, M. A. Kadhim, and ..., "Study the spatial distribution of soil properties and their relationship to the spectral indices computed from the satellite image data.," *International Journal of …*, 2021, [Online]. Available: https://search.ebscohost.com/login.aspx?direct=true&profile=ehost&scope=site&authtype=crawler&jrnl=09731903&AN=154605910&h=LQqeEbP5W4fbM4C3mOWTnfvcHYwhGpz5AKp4oWETN4Q3ufMTjJKoV9HUiQ879cDlL1rCQznaqkOqMdLSw5xU4Q%3D%3D&crl=c

[9] W. Wu, "Atmospheric Correction for Landsat Data – Material for remote sensing training," *ICARDA*, 2011.

[10] J. A. Coblinski, É. Giasson, J. A. M. Demattê, A. C. Dotto, and ..., "Prediction of soil texture classes through different wavelength regions of reflectance spectroscopy at various soil depths," *Catena (Amst)*, 2020, [Online]. Available: https://www.sciencedirect.com/science/article/pii/S0341816220300345

[11] J. A. M. Demattê, M. R. Alves, F. S. Terra, and ..., "Is it possible to classify topsoil texture using a sensor located 800 km away from the surface?," *Revista Brasileira de …*, 2016, [Online]. Available: https://www.scielo.br/j/rbcs/a/TrjCBy6NPHnjRHXX5pXcxQS/?lang=en

[12] R. K. Abdullatiff, "RELATIONSHIP OF SPECTRAL REFLECTANCE AND NDVI TO SOME SOIL PROPERTIES OF BRICKS FACTORIES SOILS IN NAHRAWAN AREA, BAGHDAD IRAQ," *Iraqi Journal of Agricultural Sciences*, 2019, [Online]. Available: https://www.jcoagri.uobaghdad.edu.iq/index.php/intro/article/view/696

[13] E. S. Mohamed, A. M. Saleh, A. B. Belal, and A. A. Gad, "Application of near-infrared reflectance for quantitative assessment of soil properties," *The Egyptian Journal of …*, 2018, [Online]. Available: https://www.sciencedirect.com/science/article/pii/S1110982317300327

[14] R. S. Dwivedi, *Remote sensing of soils*. Springer, 2017. doi: 10.1007/978-3-662-53740-4.

[15] F. Castaldi, "Sentinel-2 and Landsat-8 multi-temporal series to estimate topsoil properties on croplands," *Remote Sens (Basel)*, 2021, [Online]. Available: https://www.mdpi.com/2072-4292/13/17/3345

[16] Y. Zeng, D. Hao, A. Huete, B. Dechant, J. Berry, and ..., "Optical vegetation indices for monitoring terrestrial ecosystems globally," *Nature Reviews Earth & …*, 2022, [Online]. Available: https://www.nature.com/articles/s43017-022-00298-5

[17] ArcGIS, "Enterprise," Enterprise GIS Mapping Platform. [Online] Available at: https://www.esri.com/about/newsroom/arcnews/the-arcgis-platform-in-2014/

[18] D. G. Sullivan, J. N. Shaw, and ..., "IKONOS imagery to estimate surface soil property variability in two Alabama physiographies," *Soil Science Society of …*, 2005, doi: 10.2136/sssaj2005.0071.

[19] B. Rasti, "Feature Extraction for Hyperspectral Imagery: The Evolution from Shallow to Deep: Overview and Toolbox," *IEEE Geosci Remote Sens Mag*, vol. 8, no. 4, pp. 60–88, 2020, doi: 10.1109/MGRS.2020.2979764.

[20] A. Vallenari, "Gaia Data Release 3: Summary of the content and survey properties," *Astron Astrophys*, vol. 674, 2023, doi: 10.1051/0004-6361/202243940.

[21] P. Gholami, "Facile hydrothermal synthesis of novel Fe-Cu layered double hydroxide/biochar nanocomposite with enhanced sonocatalytic activity for degradation of cefazolin sodium," *J Hazard Mater*, vol. 381, 2020, doi: 10.1016/j.jhazmat.2019.120742.

[22] Y. Wang, "Electrical tuning of phase-change antennas and metasurfaces," *Nat Nanotechnol*, vol. 16, no. 6, pp. 667–672, 2021, doi: 10.1038/s41565-021-00882-8.

[23] F. Luo, "Dimensionality Reduction with Enhanced Hybrid-Graph Discriminant Learning for Hyperspectral Image Classification," *IEEE Transactions on Geoscience and Remote Sensing*, vol. 58, no. 8, pp. 5336–5353, 2020, doi: 10.1109/TGRS.2020.2963848.

[24] R. C. Wiens, "The SuperCam Instrument Suite on the NASA Mars 2020 Rover: Body Unit and Combined System Tests," *Space Sci Rev*, vol. 217, no. 1, 2021, doi: 10.1007/s11214-020-00777-5.

[25] A. Sinyuk, "The AERONET Version 3 aerosol retrieval algorithm, associated uncertainties and comparisons to Version 2," *Atmos Meas Tech*, vol. 13, no. 6, pp. 3375–3411, 2020, doi: 10.5194/amt-13-3375-2020.

[26] F. Huang, "Comparisons of heuristic, general statistical and machine learning models for landslide susceptibility prediction and mapping," *Catena (Amst)*, vol. 191, 2020, doi: 10.1016/j.catena.2020.104580.

[27] D. E. Shean, "A Systematic, Regional Assessment of High Mountain Asia Glacier Mass Balance," *Front Earth Sci (Lausanne)*, vol. 7, 2020, doi: 10.3389/feart.2019.00363.

[28] B. Li, "Above-ground biomass estimation and yield prediction in potato by using UAV-based RGB and hyperspectral imaging," *ISPRS Journal of Photogrammetry and Remote Sensing*, vol. 162, pp. 161–172, 2020, doi: 10.1016/j.isprsjprs.2020.02.013.

[29] S. Mansour, "Monitoring land use and land cover changes in the mountainous cities of Oman using GIS and CA-Markov modelling techniques," *Land use policy*, vol. 91, 2020, doi: 10.1016/j.landusepol.2019.104414.

[30] S. Ji, "Landslide detection from an open satellite imagery and digital elevation model dataset using attention boosted convolutional neural networks," *Landslides*, vol. 17, no. 6, pp. 1337–1352, 2020, doi: 10.1007/s10346-020-01353-2.